14th AIAA/CEAS Aeroacoustics Conference (29th AIAA Aeroacoustics Conference)
5 - 7 May 2008, Vancouver, British Columbia Canada

AIAA 2008-3061

Optimization of Fan Flow Deflection for Supersonic Turbofan Engines

Preben E. Nielsen* and Dimitri Papamoschou†
University of California, Irvine, CA 92697, USA

This study involves the application of fan flow deflectors for suppression of jet noise from low-bypass turbofan engines for next-generation supersonic aircraft. Experiments using canonical vane deflectors seek to establish correlations between aerodynamics, distortion of the mean velocity field in the jet plume, and noise reduction. The maximum radial velocity gradient, as a function of axial distance and azimuth angle, is used to quantify distortions of the plume. Vanes mounted at low azimuth angles (with respect to the downward vertical) reduce gradients in the downward direction, while vanes mounted at high azimuth angles reduce gradients in the sideline reduction. There is a significant correlation between gradient reduction and noise suppression in the azimuthal direction of the gradient. In addition, it is found that vanes with cambered airfoils perform better than vanes with symmetric airfoils. The trends obtained were used in the successful design of deflector configurations consisting of two pairs of vanes which resulted in cumulative peak overall sound pressure level (OASPL) and effective perceived noise level (EPNL) reductions of 8.8 dB and 6.7 dB respectively.

Nomenclature

A	=	nozzle exit area
c	=	vane chord length
c_L	=	lift coefficient
c_D	=	drag coefficient
D_f	=	nozzle fan diameter
f	=	frequency
G	=	radial velocity gradient
k	=	turbulent kinetic energy
M	=	Mach number
NPR	=	nozzle pressure ratio
r	=	radial direction
Re	=	Reynolds number
Sr	=	Strouhal number = $f D_f / U_p$
U	=	nozzle exit velocity
u	=	mean axial velocity in jet plume
x	=	axial direction
y	=	vertical direction
z	=	horizontal transverse direction
α	=	angle of attack
θ	=	polar angle
φ	=	azimuth angle

Subscripts

base	=	baseline reference nozzle
max	=	maximum

* Graduate Researcher, Department of Mechanical and Aerospace Engineering, nielsenp@uci.edu, AIAA Student Member.
† Professor, Department of Mechanical and Aerospace Engineering, dpapamos@uci.edu, AIAA Associate Fellow.

mic	=	microphone
p	=	primary (core) exhaust
s	=	secondary (fan) exhaust
TE	=	trailing edge
vane	=	internal fan flow deflection vane

I. Introduction

SUPERSONIC transportation is becoming increasingly viable both technologically and economically. However, a major obstacle continues to be the problem of jet noise and the regulations governing the amount of noise that can be produced near airports. This research aims to develop innovative jet noise reduction techniques for application on future civilian and military supersonic aircraft to facilitate environmental noise compliance. The primary focus of the investigation is on the design, characterization and optimization of methods to reduce overall jet noise radiation towards airport communities. This is achieved through investigation of the interconnected elements of engine cycle, aerodynamic performance and noise reduction through the use of passive-control methods to asymmetrically reshape the exhaust plume and reduce downward emitted noise, Figure 1. In this investigation fan flow deflectors[1,2] are used to achieve mean flow distortion of the supersonic jet plume. The aircraft envisioned has a cruise Mach number of 1.6 and weighs in the neighborhood of 90,000 kg.

The first phase of this work[3] identified an engine cycle with bypass ratio BPR = 2.7 and fan pressure ratio FPR = 2.2 as promising for this type of aircraft. Subscale aeroacoustic experiments simulated the exhaust conditions of this cycle and tested a variety of fan flow deflectors. Reductions in Effective Perceived Noise Level (EPNL) of as much as 4.5 dB were measured. In addition, mean flow measurements showed a tentative correlation between reduction of noise and reduction in mean velocity gradients in the azimuthal direction of the noise. In this work we seek to establish firmer correlations between the aerodynamics of the fan flow deflectors, distortion of the mean flow field, and the noise reduction. These are critical ingredients for optimization of this method.

The distortion of the mean flow field is quantified in terms of the change in the peak value of the radial velocity gradient in specific azimuthal directions and specific axial locations in the jet. Denoting the peak radial velocity gradient as $G_{\max}(x,\phi)$, we seek correlations between $G_{\max}$ and noise emission quantified either as overall sound pressure level (OASPL) or intensity within a certain 1/3-octave band (full-scale). The rationale for using $G_{\max}$ as a noise correlation parameter is that it governs the production rate of turbulent kinetic energy k. Reducing $G_{\max}$ we expect a reduction in the growth rate of k. Given that the jet has a finite axial extent, it is thus possible to reduce k throughout the underside of the jet. In turn, reducing k is expected to reduce the noise source. In prevailing empirical jet noise models[4] the noise source term dependence on turbulent kinetic energy is as strong as $k^{7/2}$, which roughly speaking means that a 20% reduction in k leads to a 3-dB reduction in noise. Past experiments[5] and computations[6] in dual-stream nozzles with fan flow deflectors have shown reduced values of k on the underside of the jet. Importantly, the experiments have shown a correlation between $G_{\max}$ and k near the end of the potential core of the jet[5]. It is important to note that the fan flow deflectors reduce $G_{\max}$ by a subtle redirection of the fan steam relative to the core stream. This process does not involve the creation of strong axial vorticity (such as in chevrons) whose interaction with turbulence is suspected to generate additional noise sources[4].

To understand the connection between aerodynamics, mean flow distortion, and acoustics, we use a simple deflector consisting of a single pair of vanes (2V) and test a variety of vane airfoils, azimuth angles, attack angles, and trailing edge positions. For the particular nozzle used here, because of its very thin fan duct, the 2V deflector does not achieve large mean-flow distortion so the noise benefit is limited. However, it enables a canonical study for establishing trends that can then be used in more complex, and more powerful, deflector arrangements.

II. Nozzle and Fan Flow Deflectors

The nozzle design in this study is based on the NASA GRC 3BB separate-flow nozzle, nominally for bypass ratio BPR = 5. The fan duct was reduced in diameter to produce BPR = 2.7 at the conditions specified by the engine cycle analysis given by the “Acoustic Tests” column of Table 1, and the entire nozzle was scaled down by factor of eight to fit within the flow rate capability of the UCI facility. The nozzle construction and coordinates of the nozzle are shown in Figure 2. The baseline nozzles were fabricated using a rapid prototyping epoxy method. The fan exit diameter was D_f = 28.1 mm, and the fan exit height was 1.8 mm.

Fan flow deflection is achieved through the use of internal airfoil-shaped vanes. The small fan exit height necessitated the fabrication of vanes of very small dimensions, of the same order as the fan exit height. The vanes were micro-machined from high-strength polycarbonate material using CAD/CAM facilities at U.C. Irvine (Roland MDX-40 Subtractive Rapid Prototyping Milling machine). Refinements in the manufacturing method of the vanes have lead to a higher accuracy product than previous studies. The vane cross sections encompassed symmetric and asymmetric airfoils. The symmetric vanes have a NACA 0012 airfoil cross section (Figure 3) while two cambered vanes were tested with NACA 4412 (Figure 4) and NACA 7514 (Figure 5) cross sections. The base and tip of each vane are shaped to conform to the geometry of the fan and core ducts at the exact location where the vane is attached. The vane chord length was 3 mm and the vane trailing edge was nominally situated 2 mm upstream of the nozzle exit. Using one-dimensional theory it is estimated that the Mach numbers at the leading and trailing edges of the vane were 0.4 and 0.8, respectively. Nozzles were tested with both single-pair and two-pair vane configurations at various azimuth angles and angles of attack.

III. Aeroacoustic Testing

Aeroacoustic tests were conducted in U.C. Irvine's Jet Aeroacoustics Facility, depicted in Figure 6. This is a subscale facility (approximately 1/40th of full scale for the tests in question) that uses helium-air mixtures for simulating the exhaust velocity and density of hot jets.[7] The exit flow conditions matched the conditions listed in the "Acoustic Tests" column of Table 1.

Jet noise was recorded by a microphone array consisting of eight 3.2 mm condenser microphones (Bruel & Kjaer, Model 4138) arranged on a circular arc centered at the vicinity of the nozzle exit. The polar aperture of the array is 30° and the array radius is 1 m. The angular spacing of the microphones is logarithmic. The entire array structure was rotated around its center to place the array at the desired polar angle. Positioning of the array is performed remotely using a stepper motor. An electronic inclinometer displayed the position of first microphone. Variations of the azimuth angle are possible by rotating the nozzle. This study encompassed the azimuth angles of 0° (downward) and 60° (sideline).

The arrangement of the microphones inside the anechoic chamber, and the principal electronic components, are shown in Figure 6. The microphones were connected, in groups of four, to two amplifier/signal conditioners (Bruel & Kjaer, Model 4138) with low-pass filter set at 300 Hz and high-pass filter set at 100 kHz. The four-channel output of each amplifier was sampled at 250 kHz per channel by a multi-function data acquisition board (National Instruments PCI-6070E). Two such boards, one for each amplifier, were installed in a Pentium 4 personal computer. National Instruments LabView software was used to acquire the signals.

The sound pressure level spectrum was corrected for actuator response, free-field correction, and atmospheric absorption. The overall sound pressure level (OASPL) was obtained by integrating the corrected spectrum. The sound spectra are corrected for the frequency response of the microphone and for atmospheric absorption. Through an elaborate procedure, the sound measurements are converted into effective perceived noise level (EPNL) measured by ground observation points. A full discussion of the noise calculation process is presented by Papamoschou.[1] The EPNL is evaluated for a constant-altitude flyover (1500-ft altitude) in the downward (φ_{mic} = 0°) and sideline (φ_{mic} = 60°) directions. In this report the PNL and EPNL are based on an engine thrust of 120.1 kN and an engine angle of attack of 10°. SPL spectra at full-scale size are presented by dividing the laboratory frequencies by the scale factor of 44 and are referenced to a distance of r/D_f =1.25 from the jet nozzle exit. The sound intensity can also be discretized into 1/3-octave bands for full scale frequencies which can also be used to determine the acoustic performance of the various fan flow deflection configurations. We present results for the 18th 1/3-octave band (f = 508 Hz, Sr = 1.16) which is very critical to human perception of noise.

IV. Mean Velocity Surveys

Each acoustic test was followed by a mean velocity survey in a duplicate dual-stream apparatus. Instead of helium-air mixtures, pure air was used in both primary and secondary streams. Therefore, the flow velocities were lower than those in the acoustic tests. However, the velocity ratio U_s/U_p = 0.67, and primary Mach number M_p = 1.03, were held the same as in the acoustic tests. The flow conditions are given by the "Mean Velocity Surveys" column of Table 1. The Reynolds number of the jet, based on fan diameter, was 0.92×10^6 in the acoustic tests and 0.47×10^6 in the mean velocity surveys.

The mean axial velocity in the jet plume was surveyed using a Pitot rake system, shown in Figure 7. The rake consists of five 1-mm internal diameter Pitot probes attached to a three dimensional traverse system. The 70 mm long probes are spaced vertically 10 mm apart using a streamlined mounting plate. Each Pitot probe is connected individually to a Setra Model 207 pressure transducer. The pressure was sampled at a rate of 1000 Hz by an analog to digital data acquisition board (National Instruments PCI-MIO-16E). Mach number and velocity were calculated from the Pitot pressure assuming constant pressure (equal to ambient value) and constant total temperature (equal to room temperature).

The three dimensional traverse system consists of three IMS MDrive 23 motor drivers connected individually to THK LM Guide Actuators. The traverse system is run remotely using National Instruments LabView over a pre-specified traverse array. The traverse array typically consisted of 28 axial planes spanning 14 inches, each axial plane comprising 17 horizontal passes of length 101.6 mm spaced 2.5 mm vertically apart. The horizontal passes were made at a speed of 10.16 mm/s.

The data on each y-z plane are interpolated on a fixed grid. The Pitot pressure is converted to velocity under the assumption of constant static pressure (equal to the ambient value) and constant total temperature (equal to room temperature). Smoothing of the velocity profiles, and computation of the velocity gradients, is performed using a Savitzky-Golay filter.

For each axial station, the radial derivatives were calculated on the radial-azimuthal ($r - \varphi$) coordinate system, Figure 8. The origin of the ($r - \varphi$) system is defined as the centroid of the region where the Pitot pressure exceeds 95% of its maximum value. The first and second derivatives were calculated along radial lines from φ=0 to 354° in increments of 4°. The resulting radial velocity gradient is normalized in the form

$$G(x,r,\phi) = \frac{D_f}{U_p}\frac{\partial u(x,r,\phi)}{\partial r}$$

Of particular interest is the maximum value of the magnitude of the gradient for given x and φ,

$$G_{\max}(x,\phi) = \frac{D_f}{U_p}\left|\frac{\partial u(x,r,\phi)}{\partial r}\right|_{\max}$$

V. Aeroacoustic Results

A parametric study was performed using a single pair of vanes placed at various azimuth angles and at angles of attack, given by Table 2. A single pair of vanes placed symmetrically about the nozzle vertical axis was employed in order to isolate the effect of the individual vane without influence from other sets of vanes or wedges as used in previous studies. Vanes with symmetric NACA 0012 airfoil sections (2V-S), cambered NACA 4412 airfoil sections (2V-C) and highly cambered NACA 7514 sections (2V-HC) were tested at azimuth angles of φ_{vane} = 50°, 90°, 120°, 150° and 165° in order to fully quantify the effect of vane azimuth angle and airfoil cross section on the aeroacoustic performance. The symmetric vanes were tested at an angle of attack α = 7.5° and the cambered NACA 4412 section vanes were placed at an angle of attack α = 4°. These angles have been shown in previous studies to give significant noise reductions for a large range of azimuth angles.[3] The highly cambered vanes were tested at an angle of attack α = 0° and α = 4°, the former having approximately the same lift coefficient c_L as the NACA 4412 airfoil at α = 4° while the latter having approximately the same drag coefficient c_D at α = 4°. An example 2-vane configuration with the vanes placed at an azimuth angle φ_{vane} = 120° is shown in Figure 9.

The aeroacoustic results for a 2-vane, φ_{vane} = 50° configuration using NACA 4412 airfoil vanes (2V-Ca) are shown in Figure 10 and Figure 11 for microphone azimuth angles φ_{mic} = 0° and φ_{mic} = 60° respectively. The aeroacoustic results are presented with respect to the baseline nozzle results. Each figure shows narrowband lossless spectra at various polar angles θ (measured from the jet axis), overall sound pressure (OASPL) versus θ, perceived noise level (PNL) versus time, and PNL versus polar angle. The reductions in EPNL and peak value of OASPL are also shown. These aeroacoustic attributes facilitate a determination of the merit of the various fan flow deflector configurations.

The 2V-Ca configuration gives large reductions in EPNL and peak OASPL for the downward direction of 2.5 dB and 2.8 dB respectively. This performance, however, is not realized in the sideline acoustic results with an increase in the EPNL of 0.1 dB and only a small decrease in the peak OASPL of 0.7 dB.

A 2-vane configuration using NACA 7514 airfoil vanes placed at an azimuth angle φ_{vane} = 120° produces the acoustic results shown in Figure 12 and Figure 13 for the downward and sideline directions respectively. The configuration presented displays significant reductions of OASPL and EPNL in both the downward direction with a microphone angle of 0° and the sideline directions with a microphone angle of 60° with a peak OASPL reduction of 2.7 dB and an EPNL reduction of 2.7 dB in the downward direction and a reduction in peak OASPL and EPNL of 2.5 dB for both metrics in the sideline direction. The highly cambered vanes with an angle of attack α = 4° produced the largest decreases in noise.

The correlations between airfoil configuration, vane azimuth angle and noise are shown for the downward direction and the sideline direction in Figure 14 and Figure 15 respectively. These correlation figures show the reduction in peak OASPL, the reduction in EPNL and the reduction in the noise intensity for the 18th 1/3 octave band for all of the 2-vane configurations tested with respect to the vane azimuth angle. The 18th 1/3-octave band corresponds to a full-scale frequency f = 508 Hz and a Strouhal number Sr = 1.16. This was chosen as a noteworthy frequency band due to its high perceived noise characteristics.

In the downward direction there is a relatively strong correlation between noise reduction and vane azimuth angle for all metrics. Vanes placed at the low azimuth angle φ_{vane} = 50° gave the best noise reductions with a steady decrease in reductions to a minimum for azimuth angles φ_{vane} = 150°. It is interesting to note that unlike the other vanes sections tested, the highly cambered NACA 7514 vanes (2V-HC1 and 2V-HC2) displayed a decrease in the 18th 1/3-octave band noise intensity (an increase in noise reduction) when the azimuth angle was increased from φ_{vane} = 90° to φ_{vane} = 120°.

A relatively strong general trend was also observed in the correlations between sideline noise and vane azimuth angle. Small noise reductions were obtained with both low and high vane azimuth angles with the largest reductions for every configuration being obtained with a vane azimuth angle φ_{vane} = 120°. In general, the configuration with the highly cambered vanes placed at an angle of attack α = 4° displayed superior noise reduction in both downward and sideline directions for most noise metrics relative to the other configurations tested.

Using the correlations obtained from the 2-vane configurations, several 4-vane configurations were tested with 2 pairs of vanes placed at a number of azimuth angles. These configurations, along with the best performing 2-vane configuration, are described in Table 3. The best performing configuration was 4V-HCa, which had pairs of vanes placed at azimuth angles φ_{vane} = 50° and φ_{vane} = 120°. This configuration resulted in significant downward peak OASPL and EPNL reductions of 4.7 dB and 3.8 dB respectively with considerable peak OASPL and EPNL reductions in the sideline direction of 4.1 dB and 2.9 dB respectively. While the peak OASPL reductions for this configuration are quite significant the slightly higher spectral sound pressure levels at the larger polar angles θ leads to marginally smaller effective perceived noise level reductions for both the downward and sideline directions.

VI. Mean Flow Results

The results for the mean flow of the jets are presented as a composite of the velocity contour for the vertical longitudinal (symmetry) plane, a number of transverse velocity contour plots at various distances downstream and several velocity line plots on the symmetry plane. Figure 19 displays the mean velocity results for the baseline nozzle. The velocity isocontours in the two planes presented are relatively axisymmetric indicating that the nozzle components (fan, core and plug) are in good alignment. The line plots also confirm this symmetry in the vertical plane. The primary potential core length, x_p, is defined as the length downstream of the plug tip at which the local maximum velocity falls to 90% of the core exit velocity. The end of the potential core is of interest as it has been identified from phased array measurements that the strongest noise sources originate from this region.[8] For the baseline case the potential core length x_p/D_f = 4.3.

The configuration consisting of a single pair of NACA 4412 airfoil vanes placed at an azimuth angle φ_{vane} = 50° (2V-Ca) produce the mean flow results shown in Figure 20 associated with the acoustic results in Figure 10 and Figure 11. A large downward distortion of the secondary stream is evident in the transverse velocity contour plots. This downward deflection is reflected in the maximum velocity contour plots in Figure 21. There is a strong decrease in maximum velocity gradient throughout the axial range of the jet centered on the downward axial direction φ = 0° and extending 10° either side. In the sideline direction φ = 60°, there is no discernable decrease in the maximum velocity gradient throughout the axial range with an increase in the maximum velocity gradient very close to the jet exit. The large reductions in downward velocity gradient and negligible change in sideline velocity gradient seem to draw a parallel to the acoustic reductions in the same directions, with significant reductions evident in the downward direction and insignificant reductions in the sideline direction, indicating the potential correlations between the gradients and the acoustic results.

The mean flow results for the configuration consisting of a single pair of NACA 7514 airfoil vanes placed at an azimuth angle φ_{vane} = 120° (2V-HCa) are displayed in Figure 22 corresponding to the acoustic results in Figure 12 and Figure 13. The addition of the vanes causes distorted cross-sections with thickening in both the downward and sideline directions. This distortion is also evident in the symmetry plane line plots. A decrease in the potential core length to x_p/D_f = 3.8 also occurs when the vanes are added which may indicate a change in the axial position of the origin of the large jet plume noise sources.

Figure 23 displays contours of maximum radial velocity gradient on the x-φ plane and the relative change in maximum velocity gradient against the baseline case. There is a significant decrease in the maximum velocity gradient for axial positions greater than x/D_f = 5.0 for azimuth angles $-60 \le \varphi \le 60$ with a peak reduction in maximum velocity gradient for φ = 0°. This reduction in maximum velocity gradient reflects the consistent decrease in peak OASPL and EPNL for the downward and sideline directions. The reduction in peak OASPL in the downward direction for this case, Figure 12, is slightly greater than the reduction in peak OASPL for the sideline direction, Figure 13, which appear to be related to the slightly higher reductions in maximum velocity gradients for the downward direction in the main reduction region for axial positions $x/D_f > 5.0$.

The mean flow result for the 4-vane configuration 4V-HCa is shown in Figure 24 corresponding to the aeroacoustic results presented in Figure 17 and Figure 18. A significant distortion of the jet plume is evident from the figure with a large low speed region being developed on the underside of the jet as a result of the two pairs of vanes and a decrease in the length of the potential core to $x_p/D_f = 3.6$. The influence of the vanes placed at the lower azimuth angle of $\varphi_{vane} = 50°$ result in a significant thickening of the jet plume in the downward direction while the vanes placed at $\varphi_{vane} = 120°$ result in a small distortion that effects the sideline direction. The maximum velocity gradient plots in Figure 25 reflect these distortions with a large decrease in the maximum velocity gradient in the downward direction for axial positions greater than $x/D_f = 4.5$ and a less significant decrease in the maximum velocity gradients in the sideline direction, again matching the trends seen in the acoustic results with better acoustic reductions in the downward than the sideline directions.

VII. Aeroacoustic – Mean Flow Correlations

In order to understand the influence of the velocity gradients on the noise that is produced in both the downward and sideline directions the maximum velocity gradient can be averaged over a certain axial range at an azimuth angle $\varphi = 0°$ for the downward direction and $\varphi = \pm 60°$ for the sideline direction. Figure 26 illustrates this process which averages the maximum velocity gradients over a specified axial range and a given azimuthal range $\Delta\varphi$ about the downward and sideline azimuth angles. This average maximum velocity gradient can then be directly related to the various noise metrics of peak OASPL, EPNL and 18th 1/3-octave band noise intensity. These correlations with the maximum velocity gradient G_{max} can be connected with the production of turbulent kinetic energy in the jet plume.

Figure 27 relates the normalized maximum velocity gradient averaged over an axial range $x/D_f = 5.4$ to 6.3 to the peak OASPL for each configuration listed in Table 2 and Table 3. A very strong correlation is realized between the averaged maximum velocity gradient and reductions in the peak OASPL in this averaging range. Other ranges investigated, while displaying similar trends did not have as strong a correlation as the results presented in Figure 27. This range is recognized as encompassing the general location of the end of the potential core, further confirming the importance of the flow field and noise sources in the vicinity of this point. It is important to note that the peak OASPL is dominated by noise emitted at Strouhal numbers $Sr \sim 0.15$.

Despite this strong correlation with the peak OASPL when the noise intensity from the 18th 1/3-octave band ($Sr = 1.16$) is presented, Figure 28 (a), as a function of normalized change in maximum velocity gradient averaged over the same region, $x/D_f = 5.4$ to 6.3, the correlation, while still present, is not as strong. This is expected because noise at $Sr = 1.1$ is expected to come from a region much closer to the jet exit. To investigate this further the noise intensity of the 18th 1/3-octave band is shown against the normalized change in maximum velocity gradient over several different axial ranges in Figure 28 (b) and Figure 28 (c). In these figures the gradient is calculated for $x/D_f =$ 3.6 to 4.5 and $x/D_f = 0.9$ to 1.8 respectively. There is only a small correlation between noise and velocity gradient in the central averaging region in Figure 28 (b), however the region close to the jet nozzle exit, Figure 28 (c), gives a very strong correlation. A notable feature is the correlation of noise suppression with gradient reduction and noise excess with gradient increase. The several sideline points which display an increase in the 18th 1/3-octave band noise correspond to the several cases where the vanes were placed at azimuth angles $\varphi_{vane} = 50°$. The velocity gradient plots in Figure 21 are typical of the $\varphi_{vane} = 50°$ configurations which display an increase in the velocity gradients in the sideline direction for azimuth angles close to the jet nozzle exit. Other configurations with the vanes placed at higher azimuth angles generally produce mean velocity profiles that have lower velocity gradients for both the sideline and the downward directions, even very close to the jet nozzle exit.

It is pertinent to note then, that while the peak OASPL is largely influenced by the velocity gradients in the vicinity of the potential core, noise sources with frequencies important to human perception (i.e., full-scale frequencies of 100 Hz and above) are influenced by velocity gradients closer to the nozzle exit. This represents a first step in a process to not only develop correlations for overall sound pressure levels but also investigate and characterize the process of noise generation at a range of frequencies at various locations in the jet plume. The obvious influence of radial velocity gradients in the jet plume and the associated changes in turbulent kinetic energy growth rate on the noise produced warrants further investigation.

VIII. Conclusion

We report an investigation of the use of passive fan flow deflectors to achieve distortion of the jet plume and reduction of noise emitted in the downward and sideline directions. Fan flow deflection was achieved through the use of internal airfoil shaped vanes and aeroacoustic and mean flow measurements were obtained for each configuration. A comprehensive parametric study of 2-vane configurations was performed with various airfoil sections, angles of attack, axial positions and azimuth angles in order to obtain correlations between the vane aerodynamics, distortion of the jet mean velocity profile and noise reduction. The noise metrics utilized in this study include overall sound pressure level (OASPL), effective perceived noise level (EPNL) and 1/3-octave noise intensity level. Of particular interest is the directional influence and effect of maximum velocity gradients in the flow field on the noise produced in the downward and sideline directions. The velocity gradients are also related to the production of turbulent kinetic energy in the jet plume. From this study several notable trends are realized:

- Vanes placed at low azimuth angles (φ_{vane} = 50°) result in superior noise reduction in the downward direction while vanes place at higher angles (φ_{vane} = 120°) give the best reductions in the sideline direction.
- There is a reasonable correlation between the noise produced and the vane azimuth angle that facilitates a suitable selection of vane positioning.
- The highly cambered vanes with a NACA 7514 airfoil section at an angle of attack α = 4° gave the largest reductions for most noise metrics utilized compared with vanes with other airfoil sections.
- A 4-vane configuration corresponding to a combination of the best performing 2-vane configurations for downward and sideline noise reduction (4V-HCa) was implemented to produce significant cumulative peak OASPL and EPNL reductions of 8.8 dB and 6.7 dB respectively.
- There is a very strong correlation between peak OASPL reduction in the downward and sideline directions and reductions in the maximum velocity gradients in these directions averaged over certain axial extents.
- Reductions in the 18th 1/3-octave band (f = 508 Hz, Sr = 1.16) are strongly correlated to directional maximum velocity gradient reductions close to the exit of the jet.
- In general reductions in noise are associated with reduced velocity gradients and noise increases with increased velocity gradients.

Acknowledgments

The support by NASA Cooperative Agreement NNX07AC62A (monitored by Mr. Tom Norum) is gratefully acknowledged. We thank Mr. An Vu for his assistance with the design and fabrication of the vanes.

References

[1]Papamoschou, D., "Fan Flow Deflection in Simulated Turbofan Exhaust," *AIAA Journal*, Vol. 44, No.12, 2006, pp. 3088-3097.

[2]Papamoschou, D., "New Method for Jet Noise Suppression in Turbofan Engines," *AIAA Journal*, Vol. 42, No.11, 2004, pp. 2245-2253.

[3]Papamoschou, D., and Nielsen, P., "Fan Flow Deflection for Supersonic Turbofan Engines," *AIAA Paper* 2008-0039, Jan. 2008.

[4]Birch, S.F., Lyubimov, D.A., Maslov, V.P., and Secundov, A.N., "Noise Prediction for Chevron Nozzle Flows," *AIAA Paper* 2006-2600, May 2006.

[5]Shupe, R.S., Zaman, K.B.M.Q., and Papamoschou, D., "Effect of Wedge-Shaped Deflectors on Flow Fields of Dual-Stream Jets," *AIAA Paper* 2007-3659, May 2007.

[6]Dippold, V., Foster, L., and Wiese, M., "Computational Analyses of Offset Stream Nozzles," *AIAA Paper* 2007-3589, May 2007.

[7]Papamoschou, D., "Acoustic Simulation of Hot Coaxial Jets Using Cold Helium-Air Mixture Jets", AIAA Journal of Propulsion and power

[8]Narayanan, S., Barber, T., and Polak, D., "High Subsonic Jet Experiments: Turbulence and Noise Generation Studies," *AIAA Journal*, Vol. 40, No. 3, 2002, pp. 430–437.

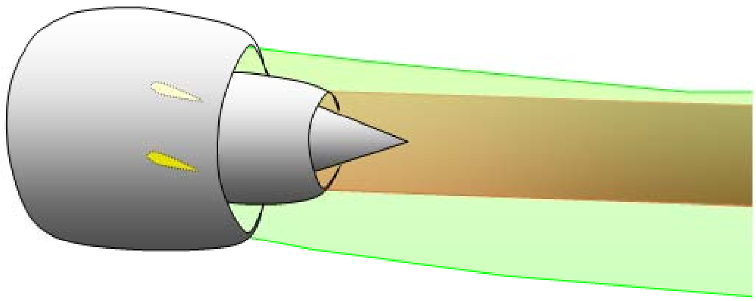

Figure 1. General concept of fan flow deflection.

Table 1. Flow conditions.

	Acoustic Tests	Mean Velocity Surveys
U_p [m/s]	600	319
M_p	1.03	1.03
NPR_s	2.00	1.96
U_s [m/s]	400	213
M_s	1.15	0.65
NPR_s	2.25	1.33
A_s/A_p	1.40	1.40
U_s/U_p	0.67	0.67

Table 2. Parametric 2-vane study configurations.

Configuration	Airfoil	x_{TE} [mm]	α [deg]	φ_{vane} [deg]
2V-S	0012	-2	7.5	50, 90, 120, 150, 165
2V-C1	4412	-1	4	50, 90, 120, 150, 165
2V-C2	4412	-2	4	50, 90, 120, 150, 165
2V-HC1	7514	-2	0	90,120
2V-HC2	7514	-2	4	90,120

Table 3. Configurations for 2-vane and 4-vane cases.

Configuration	Airfoil	x_{TE} [mm]	α_1 [deg]	φ_1 [deg]	α_2 [deg]	φ_2 [deg]
2V-Ca	4412	-2	4	50	-	-
2V-HCa	7514	-2	4	120	-	-
4V-HCa	7514	-2	4	50	4	120
4V-HCb	7514	-2	4	90	4	120
4V-HCc	7514	-2	4	90	4	150
4V-HCd	7514	-2	4	50	4	90
4V-HCe	7514	-2	4	50	4	150

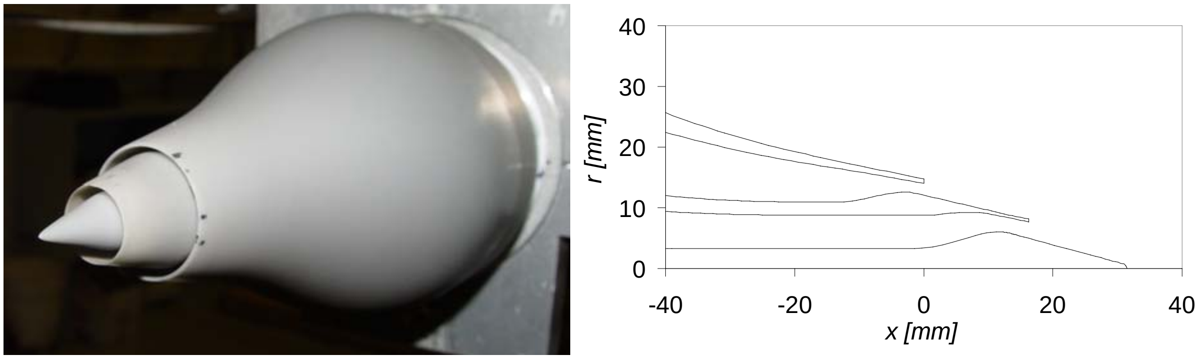

Figure 2. Assembled nozzle and coordinates of the bypass ratio BPR = 2.7 (B27) nozzle.

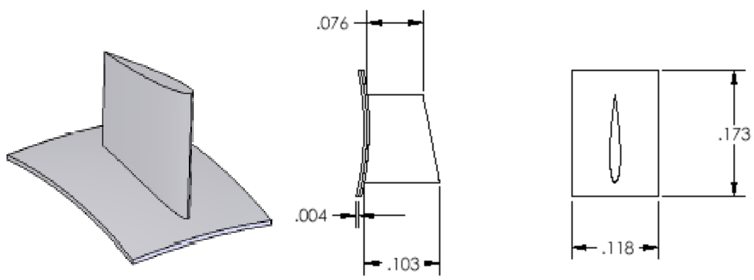

Figure 3. Design of the NACA 0012 airfoil vanes.

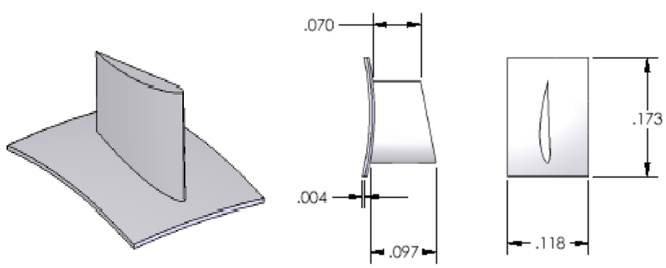

Figure 4. Design of the NACA 4412 airfoil vanes.

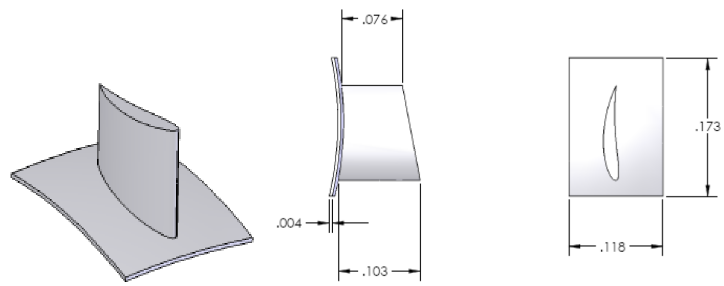

Figure 5. Design of the NACA 7514 airfoil vanes.

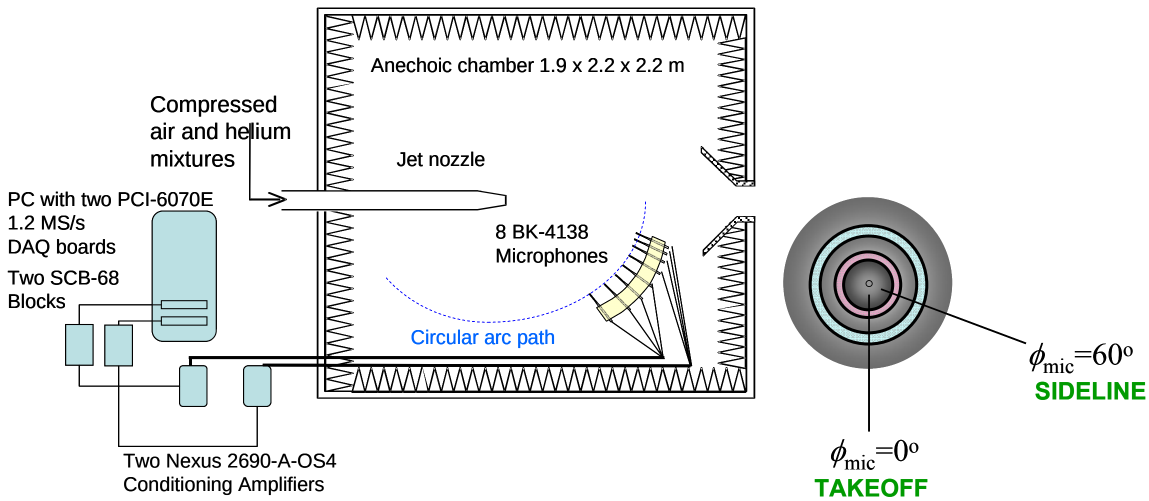

Figure 6. UCI Jet Aeroacoustics Facility and microphone azimuth angles for aeroacoustic measurement.

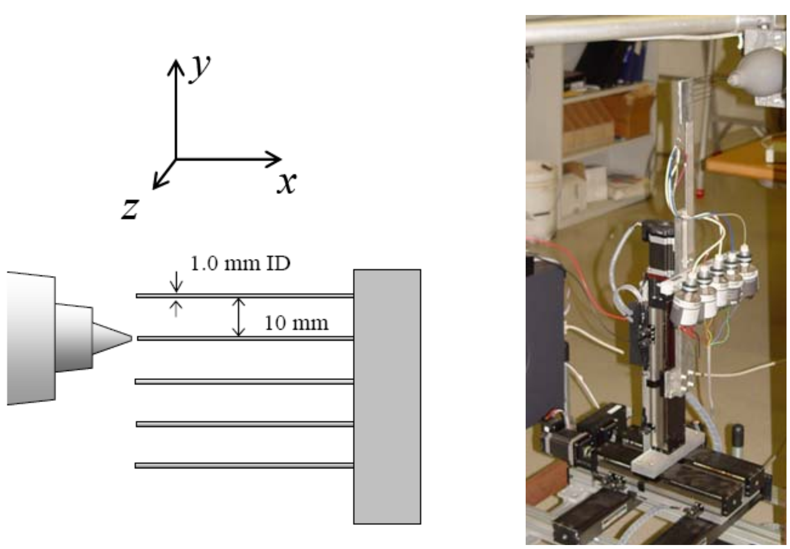

Figure 7. The Pitot traverse system for measurement of the mean velocity field.

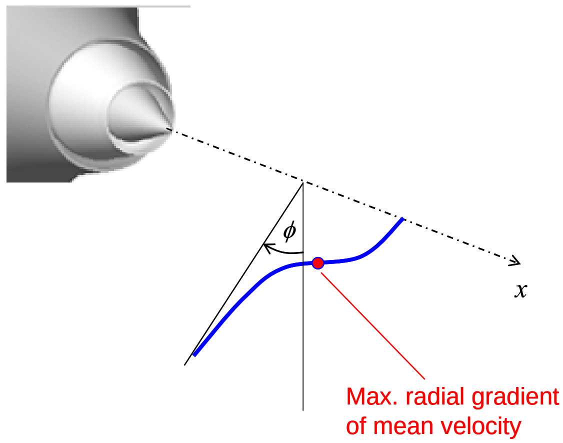

Figure 8. Illustration of maximum radial velocity gradient for each axial and azimuth position.

Figure 9. Configuration using 2 highly cambered NACA 7514 vanes at an angle of attack α = 4° and azimuth angle φ = 120° (2V-HCa).

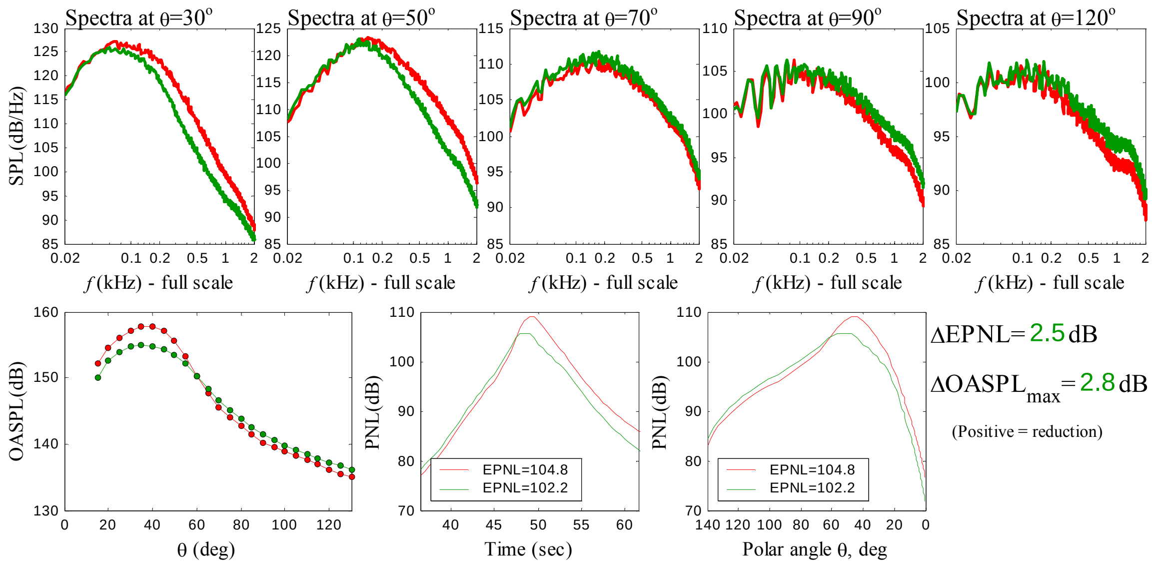

Figure 10. Acoustic results for cambered 2-vane configuration (2V-Ca) with comparison to baseline. Microphone azimuth angle φ_{mic} = 0° (downward).

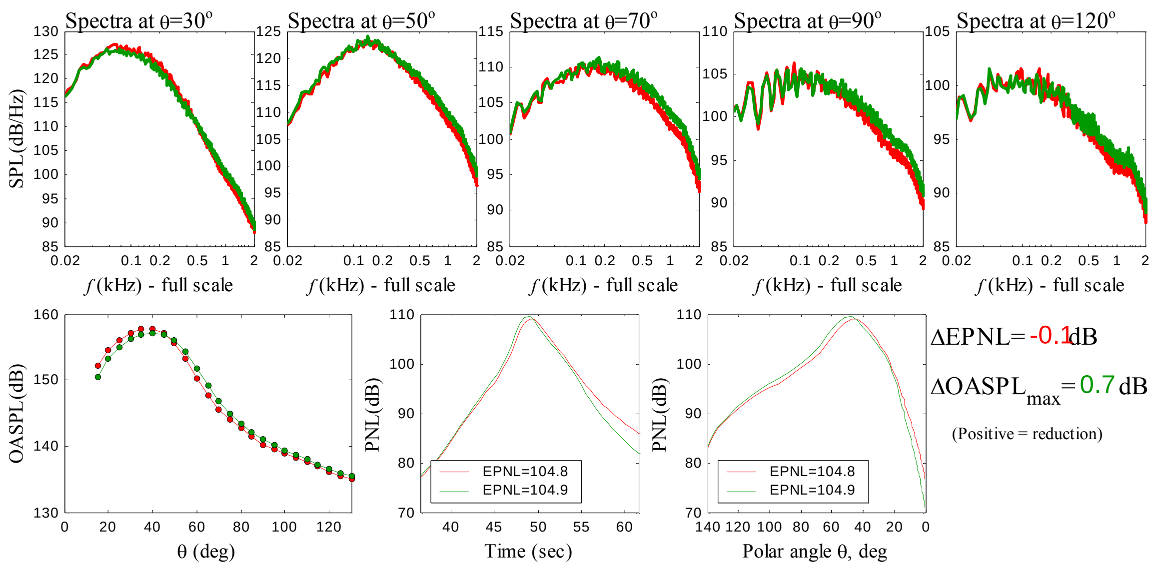

Figure 11. Acoustic results for cambered 2-vane configuration (2V-Ca) with comparison to baseline. Microphone azimuth angle φ_{mic} = 60° (sideline).

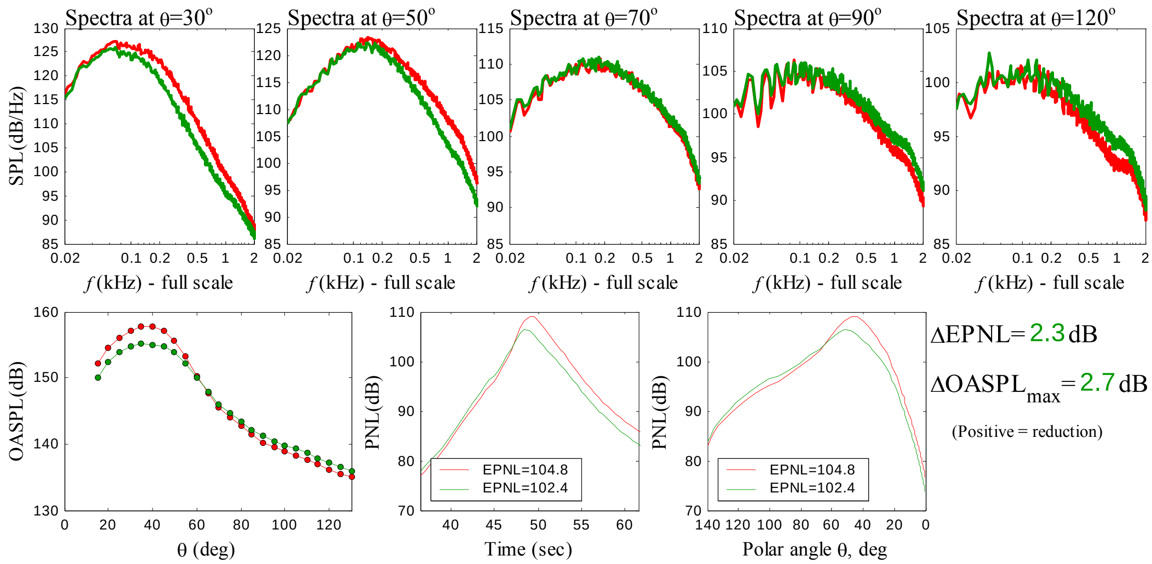

Figure 12. Acoustic results for highly cambered 2-vane configuration (2V-HCa) with comparison to baseline. Microphone azimuth angle φ_{mic} = 0° (downward).

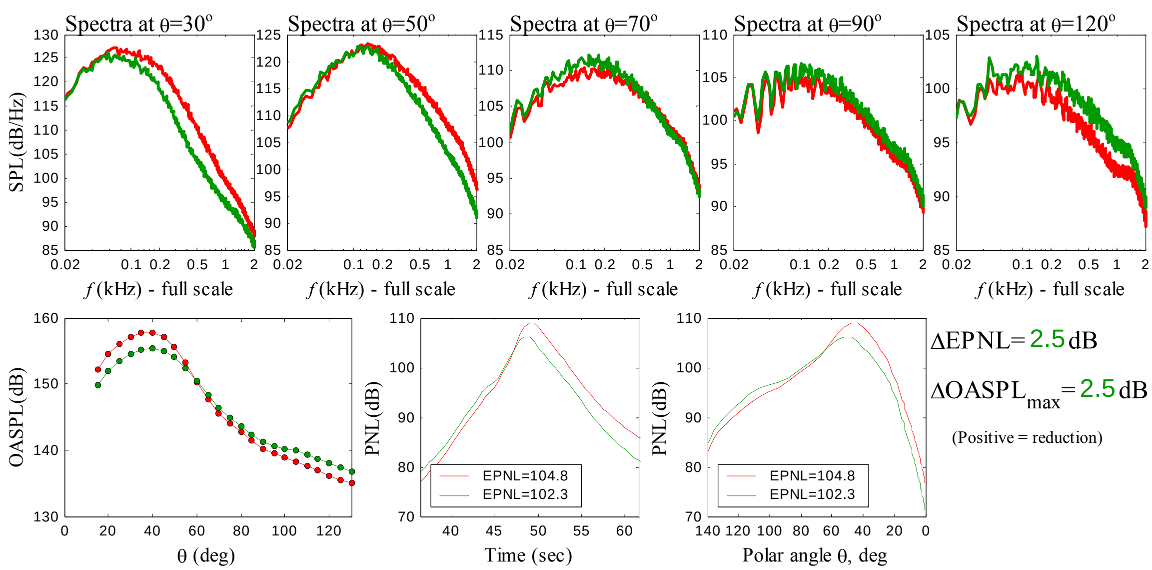

Figure 13. Acoustic results for highly cambered 2-vane configuration (2V-HCa) with comparison to baseline. Microphone azimuth angle φ_{mic} = 60° (sideline).

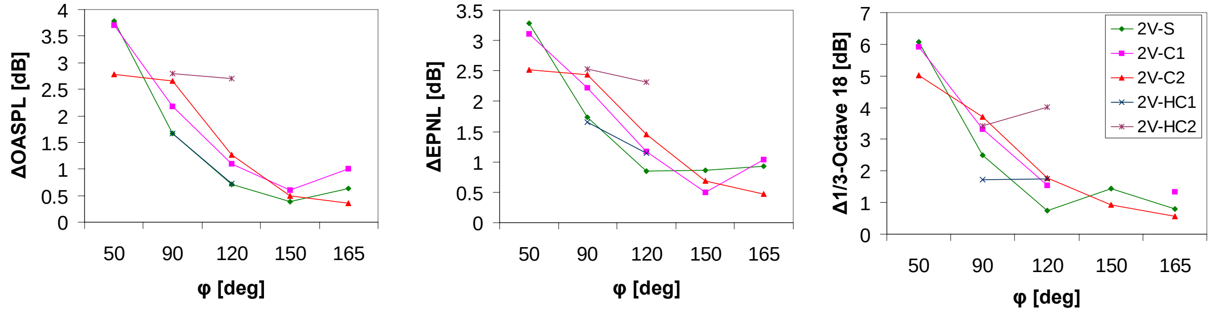

(a) (b) (c)

Figure 14. Correlation between vane azimuth angle φ_{vane} and reductions in (a) OASPL, (b) EPNL and (c) 18th 1/3-octave band in the downward direction.

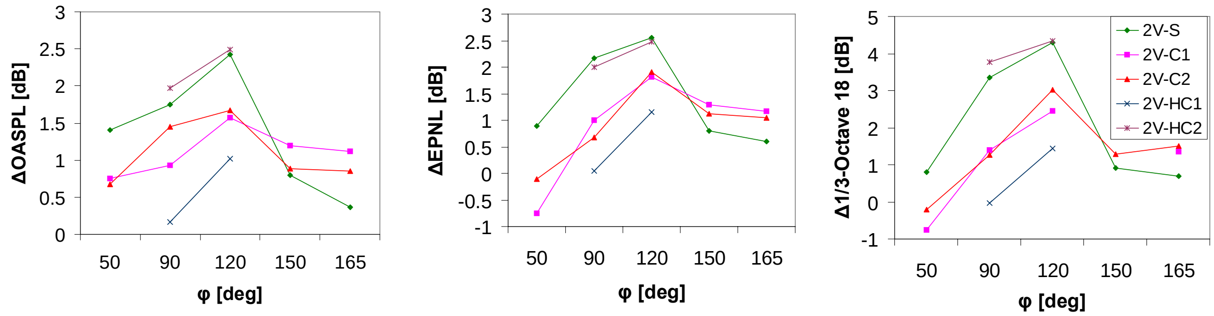

(a) (b) (c)

Figure 15. Correlation between vane azimuth angle φ_{mic} and reductions in (a) OASPL, (b) EPNL and (c) 18th 1/3-octave band in the sideline direction.

Figure 16. Configuration using 4 highly cambered NACA 7514 vanes at an angle of attack $\alpha = 4°$ and azimuth angles $\varphi_{vane} = 50°$ and $\varphi_{vane} = 120°$ (4V-HCa).

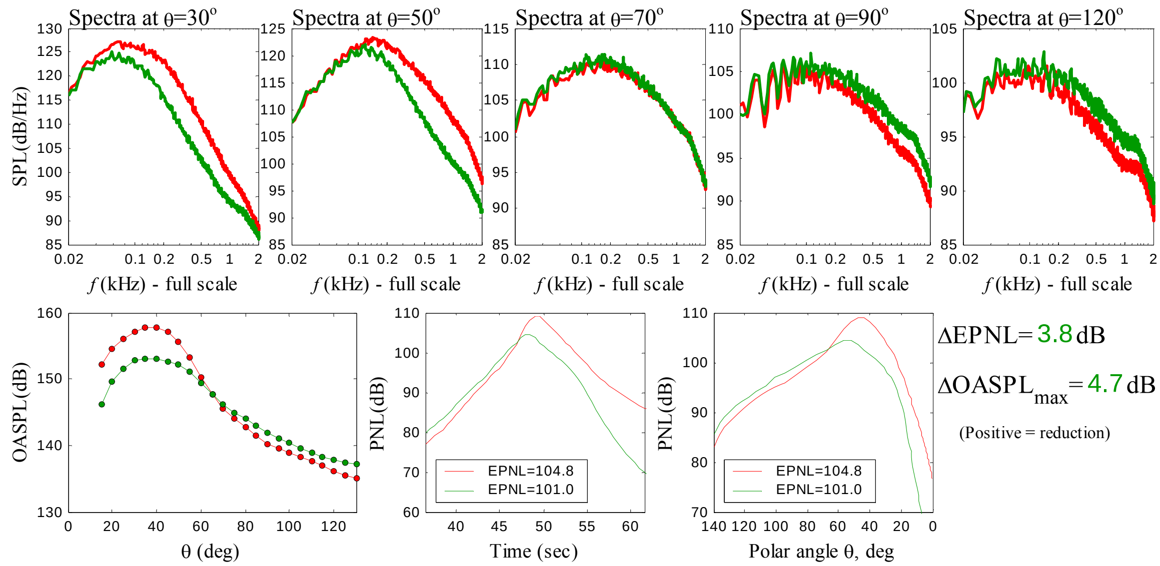

Figure 17. Acoustic results for highly cambered 4-vane configuration (4V-HCa) with comparison to baseline. Microphone azimuth angle φ_{mic} = 0° (downward).

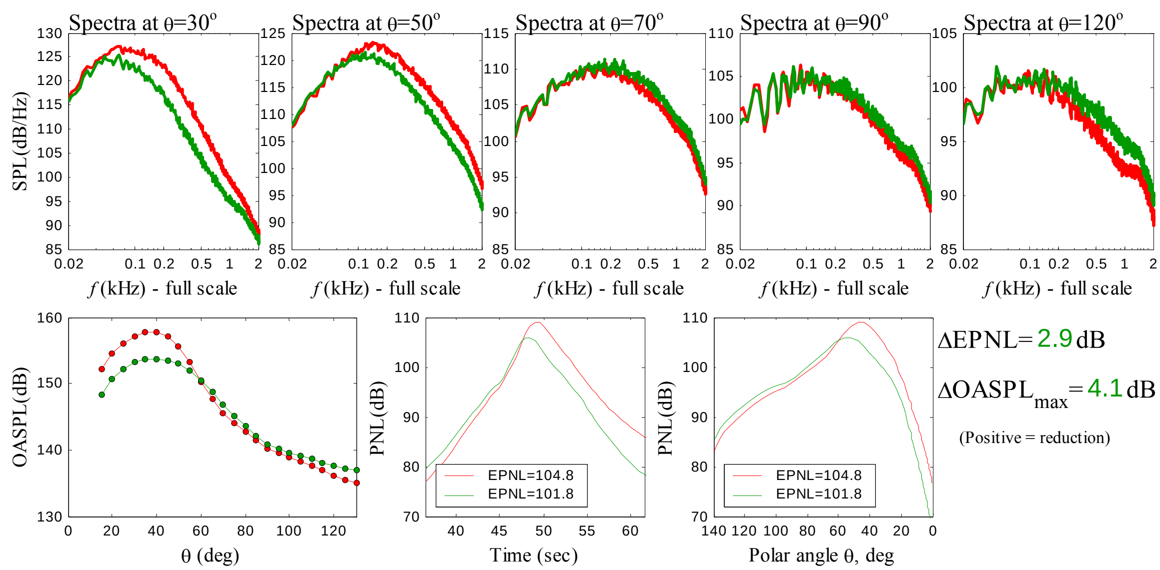

Figure 18. Acoustic results for highly cambered 4-vane configuration (4V-HCa) with comparison to baseline. Microphone azimuth angle φ_{mic} = 60° (sideline).

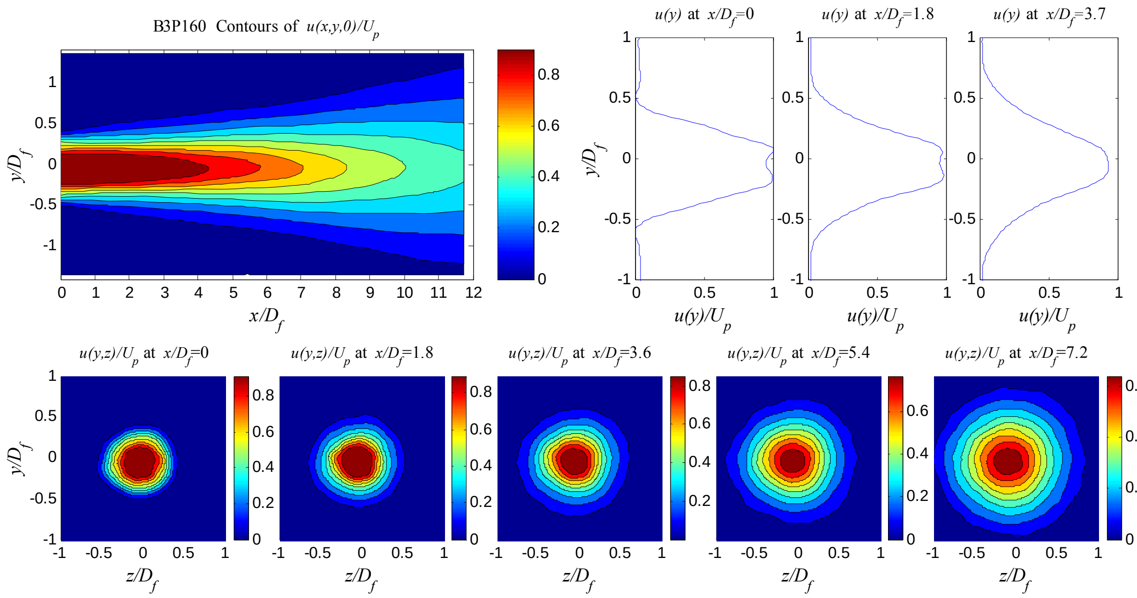

Figure 19. Mean velocity results for baseline nozzle.

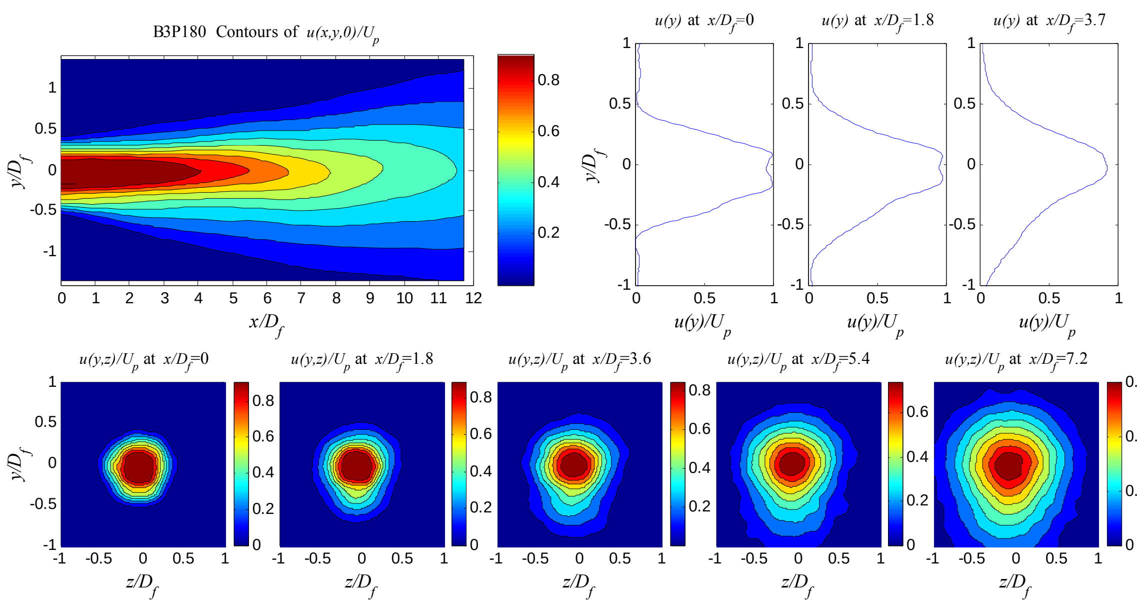

Figure 20. Mean velocity results for cambered 2-vane configuration (2V-Ca).

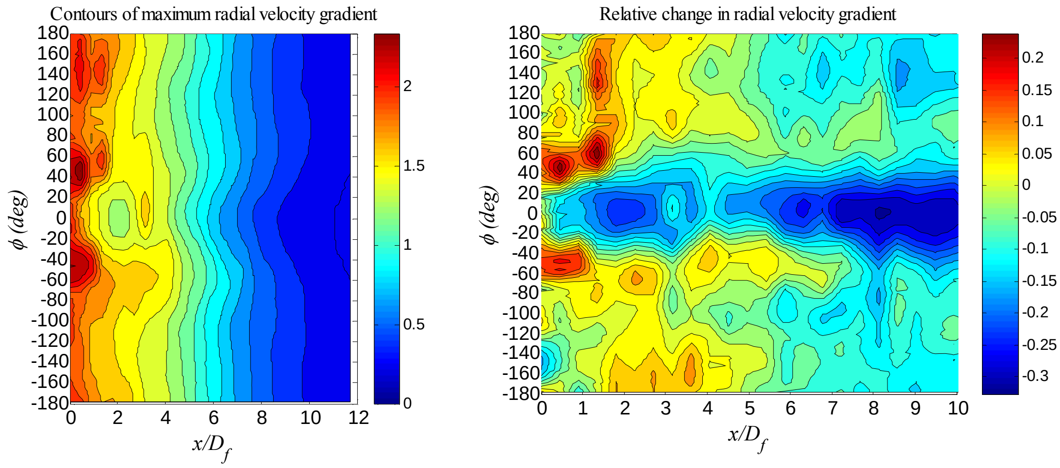

Figure 21. Contours of maximum velocity gradient on x-φ plane shown in absolute (left) and differential (right) forms for cambered 2-vane configuration (2V-Ca).

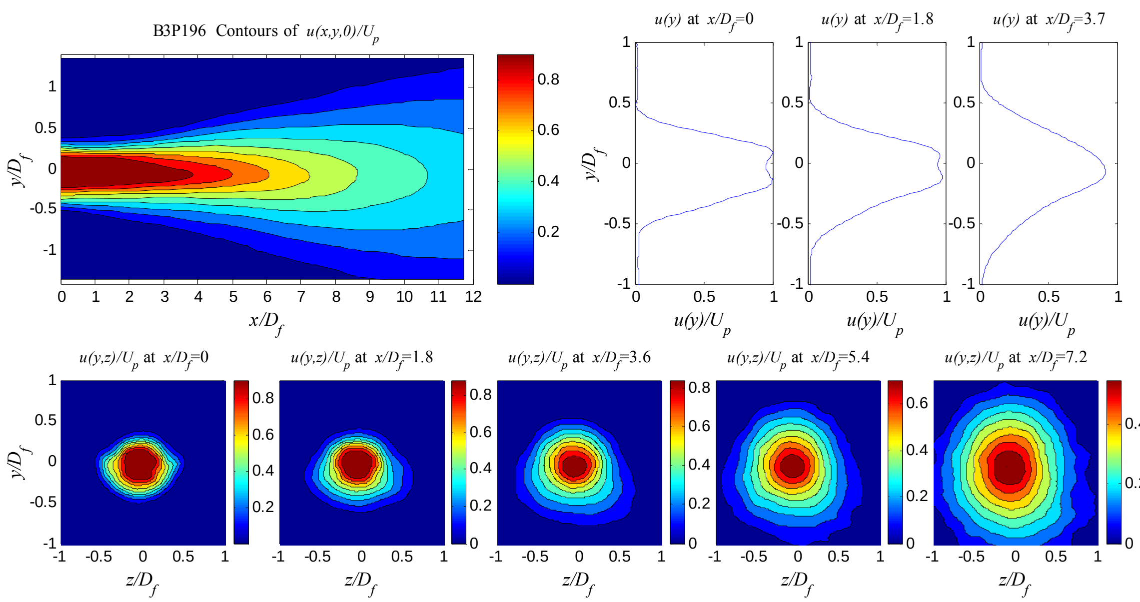

Figure 22. Mean velocity results for highly cambered 2-vane configuration (2V-HCa).

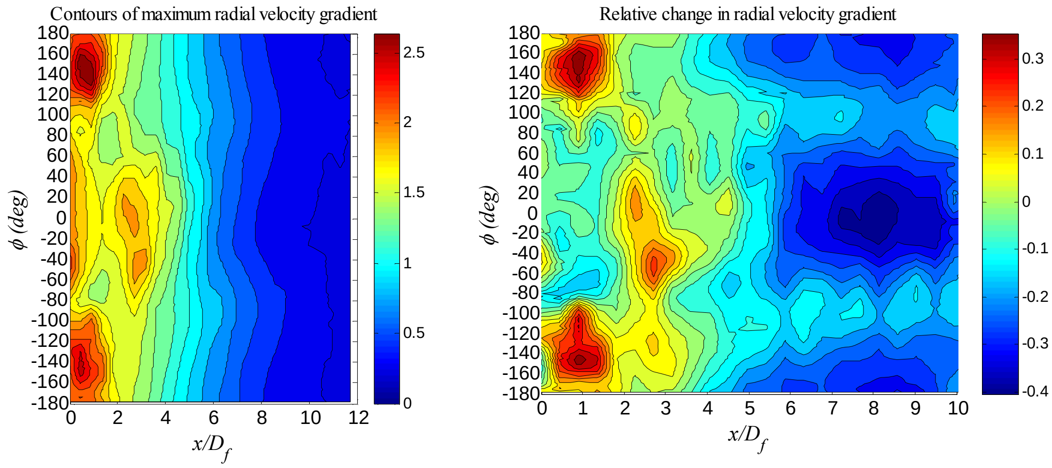

Figure 23. Contours of maximum velocity gradient on *x-φ* plane shown in absolute (left) and differential (right) forms for highly cambered 2-vane configuration (2V-HCa).

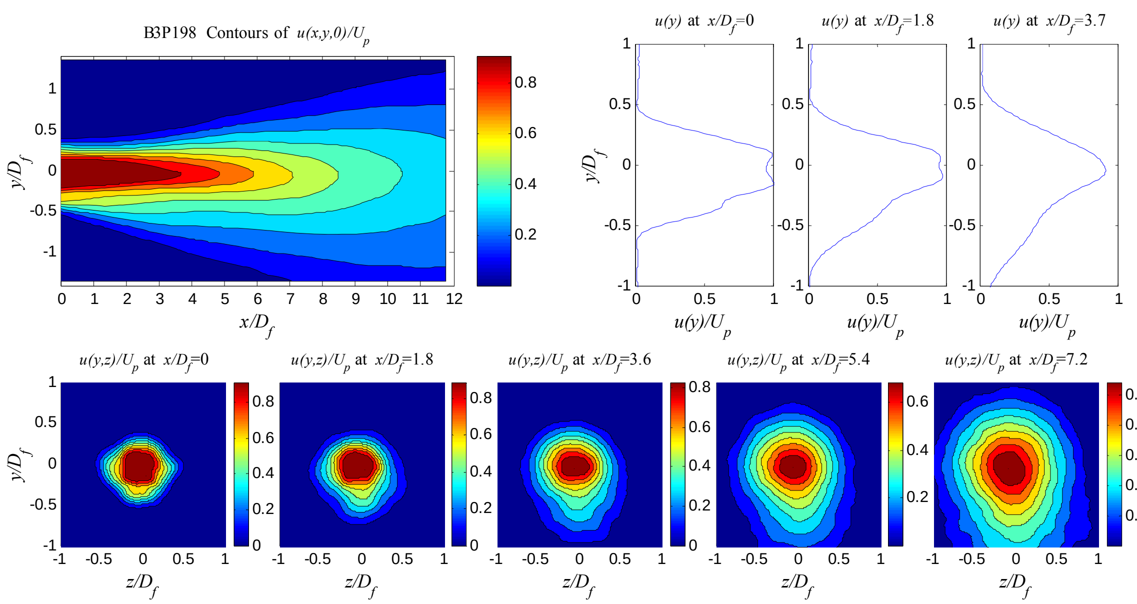

Figure 24. Mean velocity results for highly cambered 4-vane configuration (4V-HCa).

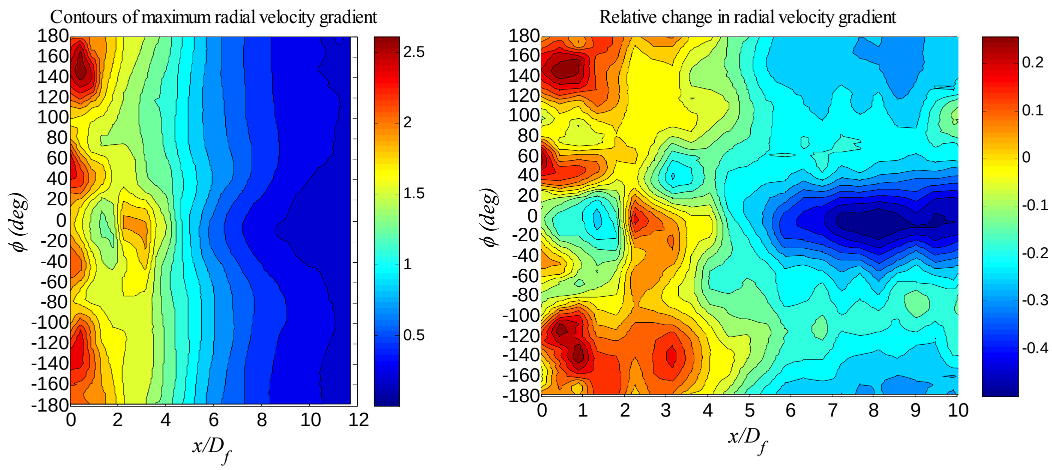

Figure 25. Contours of maximum velocity gradient on *x-φ* plane shown in absolute (left) and differential (right) forms for highly cambered 4-vane configuration (4V-HCa).

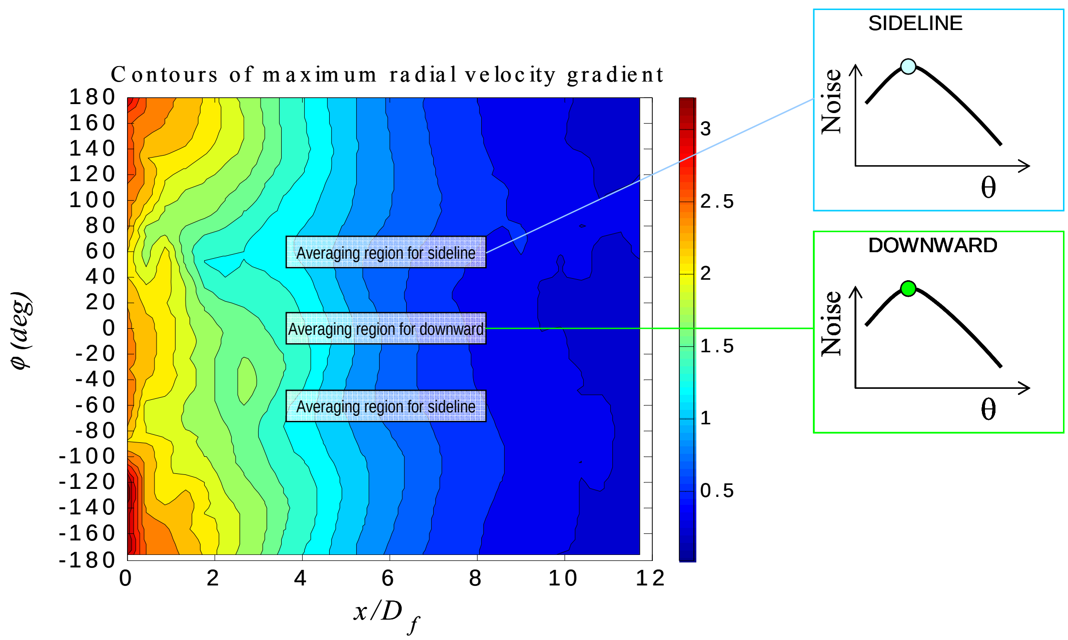

Figure 26. Correlations of averaged maximum gradient from mean velocity surveys and noise from aeroacoustic measurements.

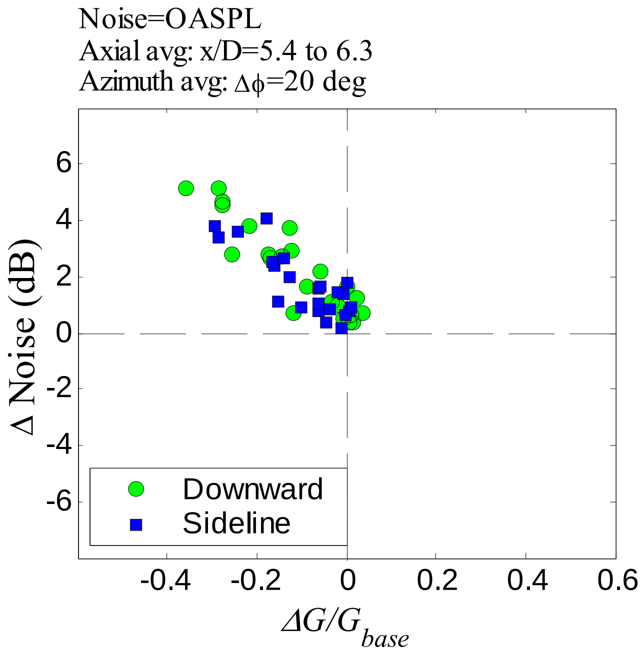

Figure 27. Correlation between peak OASPL and maximum velocity gradient averaged over x/D_f = 5.4 to 6.3 for both downward and sideline directions.

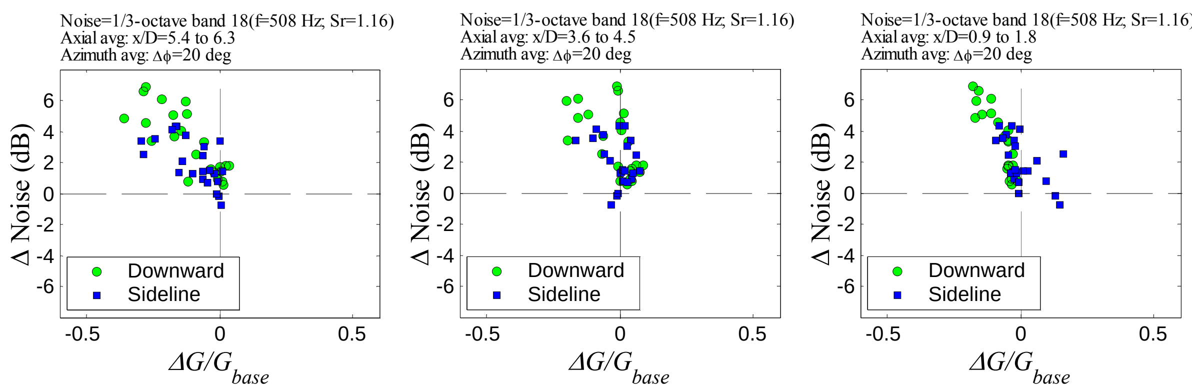

(a) **(b)** **(c)**

Figure 28. Correlation between noise and gradient for 18th 1/3-octave band averaged over (a) x/D_f = 5.4 to 6.3, (b) x/D_f = 3.6 to 4.5 and (c) x/D_f = 0.9 to 1.8.